Dynamic Maintenance and Visualization of Molecular Surfaces

Chandrajit L. Bajaj Valerio Pascucci
Department of Computer Sciences and TICAM
University of Texas, Austin, TX 78712

Robert J. Holt Arun N. Netravali
Bell Laboratories, Lucent Technologies
Murray Hill, NJ 07974

August 31, 1998

Abstract

Molecular surface computations are basic molecular modeling operations that are necessary to deal with in order to perform synthetic drug design. Computing and updating exact *boundary representations* of such molecular surfaces are critical steps that introduce for molecules the same geometric data structure used in the solid modeling community. This allows us to gain immediate access to a wide range of modeling operations/techniques that allow us to use a general solid modeling system as a molecular modeling interface: one could for example replace single atoms or entire protein bases. In this paper we introduce efficient techniques for computing NURBS (non-uniform rational B-splines) boundary representations of molecular surfaces, providing also the option of trading accuracy of the representation for the efficiency of the computation, especially in a dynamic setting. In particular we discuss two main classes of updates: one that keeps the topology of the molecular configuration fixed, and the more complicated case where the topology may be updated continuously. In general the output generated is in a representation format that can be loaded into a standard solid modeling system. It can also be directly triangulated or rendered, possibly at different levels of resolution, by a standard graphics library such as OpenGL without any additional effort.

1 Introduction

The high combinatorial complexity of macromolecules makes it challenging to compute and update their structures and properties in real time. Several different approaches have been developed to achieve this efficiency for molecular surface computations [12, 13, 38–40, 42, 43]. Other work on surface representations features the use of metaballs, molecular surfaces, and blobby models [1,8,17, 26,27,29,33–35,45–48]. In this paper we extend this work by describing algorithms that dynamically update and render exact smooth trimmed NURBS (non-uniform rational B-splines) representations for moving or growing the molecular surfaces. Trimmed NURBS are an industry-wide CAD/CAGD standard and fast becoming optimized for graphics rendering software (OpenGL)/hardware [32, 41].

In [5] we present an exact trimmed NURBS boundary representation of the Lee-Richards solvent contact molecular surface [14]. We show in this paper how this trimmed NURBS representation can be efficiently maintained to animate both the solvent accessible surface and the Lee-Richards solvent contact surface of a molecule.

In our approach we combine the use of efficient data structures [21] that have already been shown useful for molecular modeling [24] with the use of standard graphics libraries such as OpenGL and OpenInventor [44]. The basic idea is to dynamically maintain the primary structures and exactly compute and update representations (tensor product rational B-splines, trimmed NURBS) of the molecular surface which are directly displayed by optimized trimmed NURBS rendering functions of OpenGL. In particular we focus on the special case of dynamic, continuous modification of the solvent radius.

We analyze the complexity of two main classes of updates that yield a family of all the molecular surfaces obtained for different solvent radii: (1) updates that keep the Power Diagram [3] fixed (quadratic growing of the radius of the solvent ball); (2) updates that modify the Power Diagram (linear growing of the radius of the solvent ball).

In both cases efficiency is achieved trough the introduction of a novel geometric construction. In case (1) we use a new constructive approach to duality that generalizes the standard "lifting" scheme [21], showing that the Power Diagram of a molecule (3D union of balls) constitutes a compact representation of the collection of all the Power Diagrams of the trimming circles of all the patches in a molecular surface. In particular the convex cell of the 3D Power Diagram relative to the ball B is the dual of the 2D Power Diagram of the trimming circles of B. As a first approximation (with the bonus of being simpler and more efficient) we consider the molecular

surfaces obtained by disproportionally increasing the solvent radius so that the associated Power Diagram remains unchanged. We show how we can keep track of the topological changes that occur in the trimming curves of the patches that form the molecular surface so that its boundary representation can be updated efficiently. Furthermore, we compute and dynamically update an exact boundary representation of the molecular surface so that the same dynamic data-structure is also suitable for molecular modeling operations such as those supporting synthetic drug design [31].

In previous work on dynamic triangulations the focus has been mostly on the simpler Delaunay/Voronoi structures (unweighted case) [2,4,11,25,28,30,36,37]. Little has been done on the more general case of dynamic Regular Triangulation/Power Diagrams and for dimensions greater than two. Moreover, the kinds of dynamic operations developed are usually just the insertion/deletion of a single point. Such local operations become inefficient when we need to perform even a simple but global modification. Here we adopt an approach for global modifications where after a preprocessing each patch in the molecular surface is treated independently. By the "dividi et impera" paradigm we increase efficiency by solving several small problems in place of a single large one.

In the case (2) setting, where the 3D Power Diagram is subject to flips, we use the same construction as in [24] based on the definition of a 4D complex of convex polytopes $\mathcal{C}$ whose "horizontal" slices are all the possible 3D Power Diagrams of the growing balls for any growth factor r. Hence we apply a simple hyperplane sweep algorithm to optimally maintain the dynamic Power Diagram of the linearly growing balls. Thus in this case we compute exactly the offset of the union of balls (so that its topology can be precisely determined), even when it requires a change in the nearest neighbor (under power distance) relations among the atoms corresponding to flips in the associated Regular Triangulation. More generally, for a set of balls in d-dimensional space this requires the construction of a complex of convex polytopes in $(d+1)$-dimensional space whose "horizontal" slices are all the possible Power Diagrams.

In either case we prove and also demonstrate via our implementation that: (a) for small solvent radius changes the global topological structure of the molecular surface remains unaltered, requiring scaling and a dynamic maintenance of the arrangement of domain B-spline trimming curves, and (b) for large solvent radius changes, the regions in which the eventual updates of the topological structure is required is also localized. Both of the constructions are defined in general for unions of growing balls in any fixed dimension.

Our techniques are shown to be general enough to also deal with new smooth molecular surfaces [20] proposed to avoid the singularities that may arise in the Richard's rolling ball surface.

2 Dynamic Regular Triangulation and Power Diagram

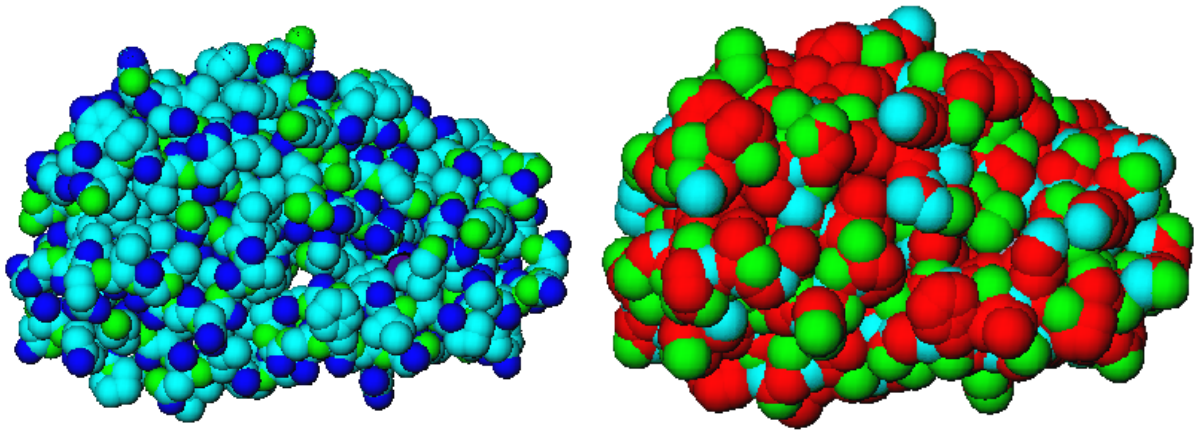

(a) (b)

Figure 1: The *HIV-2 PROTEASE* (a) and one solvent accessible surface (b) for the same molecule.

One of our goals in developing algorithms for automatically maintaining dynamic molecular surfaces is to provide means for immediate display with a standard graphics library like OpenGL without making the additional effort of triangulating the surface as in [1]. At this end we have developed [5] a boundary representation scheme where patches are standard trimmed NURBS. We show in this paper how this data structure can be efficiently maintained to animate the solvent accessible surface (see figure 1) and the solvent contact surface (see figure 2) of a molecule. In particular we focus on the special case of dynamic, continuous modification of the solvent radius[1].

2.1 Balls in $\Re^d$ and Halfspaces in $\Re^{d+1}$

In this section we introduce the fundamental equations that form the basis of the presented approach for molecular modeling. For a more extensive discussion of the conditions under which the present approach can be extended to a more general case unifying geometries other than spheres, the interested reader is referred to [7].

Consider in $\Re^{d+1}$ the implicit equation of the unit ball:

$$\xi_1^2 + \xi_2^2 + \cdots + \xi_d^2 + \xi_{d+1}^2 - 1 \leq 0 \ . \tag{1}$$

[1]See the animation in `http://www.cs.purdue.edu/research/shastra/projects/molecular/Nutrasweet_ConnollySurface/gramicidin.mpg`

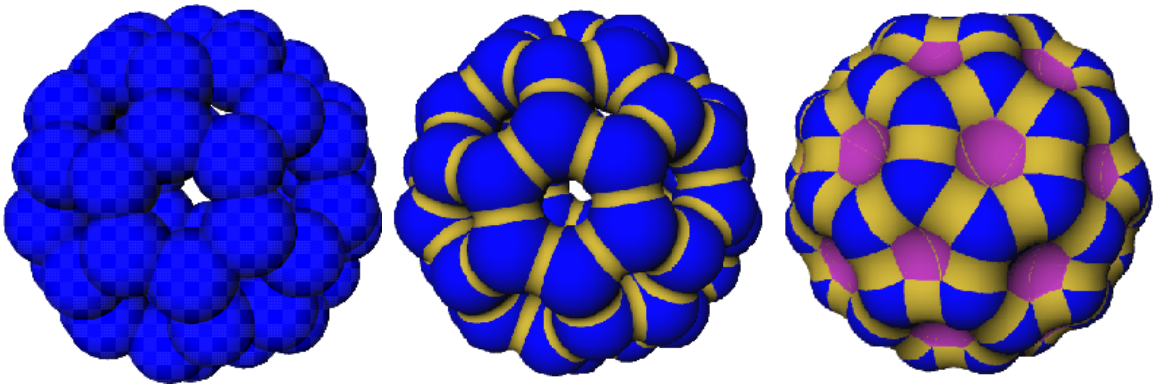

(a) (b) (c)

Figure 2: The Fullerene molecule (a) and two solvent contact surfaces (b),(c) corresponding to two different solvent radii.

Its boundary has parametric equations which are:

$$\begin{aligned} \xi_i &= \frac{2x_i}{x_1^2+\cdots+x_d^2+1}\,, \quad i=1,\ldots,d \\ \xi_{d+1} &= \frac{x_1^2+\cdots+x_d^2-1}{x_1^2+\cdots+x_d^2+1}\,. \end{aligned} \tag{2}$$

The boundary of the ball (1) is the closure of the image of $\Re^d$ in $\Re^{d+1}$ under the mapping (2). The inverse map of (2) is given by

$$x_i = \frac{\xi_i}{1-\xi_{d+1}}\,, \quad i=1,\ldots,d \tag{3}$$

for $(\xi_1,\xi_2,\ldots,\xi_d,\xi_{d+1})$ on the unit sphere $\xi_1^2+\cdots+\xi_{d+1}^2=1$. The point $(0,\ldots,0,1)$ in $\Re^{d+1}$ is the image of the point at infinity of $\Re^d$.

Consider the linear halfspace:

$$h: \quad a_0+a_1\xi_1+\cdots+a_d\xi_d+a_{d+1}\xi_{d+1}\le 0\,, \tag{4}$$

where not all of $\{a_1,\ldots,a_{d+1}\}$ are zero. Its pre-image in $\Re^d$, given by the mapping (2), is

$$b: \quad a_0(x_1^2+\cdots+x_d^2+1)+a_1\,2x_1+\cdots+a_d\,2x_d+a_{d+1}(x_1^2+\cdots+x_d^2-1)\le 0\,. \tag{5}$$

If $a_1^2+\cdots+a_{d+1}^2-a_0^2\ge 0$ and $a_0+a_{d+1}>0$, this is the ball of center $-(a_1,\ldots,a_d)/(a_0+a_{d+1})$ and radius $(a_1^2+\cdots+a_{d+1}^2-a_0^2)^{1/2}/(a_0+a_{d+1})$. If $a_1^2+\cdots+a_{d+1}^2-a_0^2\ge 0$ and $a_0+a_{d+1}<0$, this is the union of the sphere of center $-(a_1,\ldots,a_d)/(a_0+a_{d+1})$ and radius $(a_0^2-a_1^2-\cdots-a_{d+1}^2)/(-a_0-a_{d+1})$

and its exterior. When $a_0 + a_{d+1} = 0$, this is a halfspace, and when $a_1^2 + \cdots + a_{d+1}^2 - a_0^2 < 0$ and $a_0 + a_{d+1} \neq 0$, this is a ball of imaginary radius, and contains no real points.

We now examine in detail the relationship between hyperplanes in $\Re^{d+1}$ and balls in $\Re^d$. We will denote as b a ball in $\Re^d$ and B the unit ball in $\Re^{d+1}$. Also, ∂h will denote the boundary hyperplane of the halfspace h. We rewrite inequality (5) as:

$$b: \quad (a_0 + a_{d+1})(x_1^2 + \cdots + x_d^2) + 2(a_1 x_1 + \cdots + a_d x_d) + (a_0 - a_{d+1}) \leq 0 \ . \tag{6}$$

This is the ball corresponding to the halfspace:

$$h: \quad a_0 + a_1\xi_1 + \cdots + a_d\xi_d + a_{d+1}\xi_{d+1} \leq 0 \ .$$

The correspondence is given by the parametric equations (2) for the unit sphere (in $\Re^{d+1}$):

$$\partial B: \quad \xi_1^2 + \xi_2^2 + \cdots + \xi_d^2 + \xi_{d+1}^2 - 1 = 0 \ . \tag{7}$$

When (6) represents a real ball, that is when $a_1^2 + \cdots + a_{d+1}^2 - a_0^2 \geq 0$ and $a_0 + a_{d+1} > 0$, the ball b has center $-(a_1, \ldots, a_d)/(a_0 + a_{d+1})$ and radius $(a_1^2 + \cdots + a_{d+1}^2 - a_0^2)^{1/2}/(a_0 + a_{d+1})$. When $a_0 + a_{d+1} = 0$, b has infinite radius and center at infinity. In this case the inequality (6) degenerates into a halfspace. With respect to the positions of h and B we have that ∂h contains the point $(0, 0, \ldots, 0, 1)$ of B, the base point of the parameterization (2). Since we represent a ball b with $d + 2$ parameters (those of inequality (6)) instead of just $d + 1$ (center coordinates and radius) we can represent balls of any radius (even infinity or imaginary) and center in any position (finite or at infinity). This may be regarded as representing the ball in homogeneous coordinates of projective space. Explicitly, we represent the ball with center $(x_1, \ldots, x_d)$ and radius r by

$$\begin{aligned} a_0 &= 1 + x_1^2 + \cdots + x_d^2 - r^2 \\ a_i &= -2x_i \ , \quad i = 1, \ldots, d \\ a_{d+1} &= 1 - x_1^2 - \cdots - x_d^2 + r^2 \ . \end{aligned}$$

If $a_1^2 + \cdots + a_{d+1}^2 - a_0^2 = 0$ and $a_0 + a_{d+1} \neq 0$, then b is a point and ∂h is tangent to B at the point $(-a_1/a_0, \ldots, -a_{d+1}/a_0)$. If $a_1^2 + \cdots + a_{d+1}^2 - a_0^2 < 0$ and $a_0 + a_{d+1} \neq 0$, then ∂h does not intersect B. This corresponds to b having imaginary radius (in terms of weighted triangulations it is a point with negative weight). If $a_1^2 + \cdots + a_{d+1}^2 - a_0^2 > 0$ and $a_0 + a_{d+1} \neq 0$, then b has a positive radius, and ∂h intersects B in a d-disk with positive radius. If $a_0 + a_{d+1} = 0$ and not all of $\{a_1, \ldots, a_d\}$ are zero, then b is a halfspace, and ∂h intersects B at $(0, \ldots, 0, 1)$ and is not tangent

to B there. Finally, if $a_0 - a_{d+1} = 0$ and $a_1 = \cdots = a_d = 0$, then b is either all of $\Re^d$ or $\emptyset$ depending on whether $a_0 + a_{d+1} < 0$ or $a_0 + a_{d+1} > 0$, respectively, and ∂h is tangent to B at $(0, \ldots, 0, 1)$.

There are many interesting relationships between spheres in $\Re^d$ and hyperplanes in $\Re^{d+1}$. One note which should be observed is that since the mapping (2) yields only points on the unit ball in $\Re^{d+1}$, individual points in $\Re^d$ are always mapped to points satisfying (7). Thus when we speak of a mapping between a ball in $\Re^d$ and a hyperplane in $\Re^{d+1}$, this can also be interpreted as a mapping between a ball in $\Re^d$ and the intersection of the corresponding hyperplane with the unit sphere in $\Re^{d+1}$. These intersections (when they are not empty or a single point) are spheres of one lower dimension, embedded in $\Re^d$.

A fundamental relationship is that spheres that contain a point $(c_1, \ldots, c_d)$ in $\Re^d$ map to hyperplanes that pass through the point $(2c_1, \ldots, 2c_d, c_1^2 + \cdots + c_d^2 - 1)/(c_1^2 + \cdots + c_d^2 + 1)$ in $\Re^{d+1}$. This is a result of the relation

$$(c_1^2 + \cdots + c_d^2 + 1)a_0 + 2(c_1 a_1 + \cdots + c_d a_d) + (c_1^2 + \cdots + c_d^2 - 1)a_{d+1} = 0 \quad .$$

A consequence of this relationship is that a set of spheres passing through two distinct points in $\Re^d$ correspond to a set of hyperplanes in $\Re^{d+1}$ that contain a certain line. Since the actual points of intersection in $\Re^d$ are mapped to points on B, the line in $\Re^{d+1}$ must intersect B in two points. A set of spheres in $\Re^d$ which intersect at one point are mapped to into hyperplanes whose line of intersection is tangent to B. A set of spheres whose combined intersection is empty are mapped to hyperplanes whose line of intersection, if any, does not intersect B. This situation is illustrated for $d = 2$ in Figure 3. Let l be the line of intersection of the boundaries $\partial h' \cap \partial h''$ corresponding to two distinct intersecting balls b' and b''. We have that $\partial b'$ intersects $\partial b''$ if and only if l intersects B, that is, if the distance from l to the origin O is smaller than 1:

$$\partial b' \cap \partial b'' = 1 \text{ or } 2 \text{ points} \quad \Longleftrightarrow \quad l \cap B \neq \emptyset \quad \Longleftrightarrow \quad \text{dist}(l, O) \leq 1 \quad .$$

$$\dim\,(b' \cap b'') = 0 \quad \Longleftrightarrow \quad l \cap B = 1 \text{ point} \quad \Longleftrightarrow \quad \text{dist}(l, O) = 1 \quad .$$

Similarly we can consider three distinct disks b', b'', and b'''. If their intersection is a region bounded by three circular arcs, one from each disk, then the three boundary circles correspond to three planes $\partial h'$, $\partial h''$, and $\partial h'''$ that intersect in a point p contained in B. This is illustrated in Figure 4. If the three circular boundaries intersect in one or two points, then the planes intersect in a point on ∂B (or possibly in a line that intersects B).

$$b' \cap b'' \cap b''' = \text{ region bounded by 3 arcs (or points)} \quad \Longleftrightarrow \quad p \in B \tag{8}$$

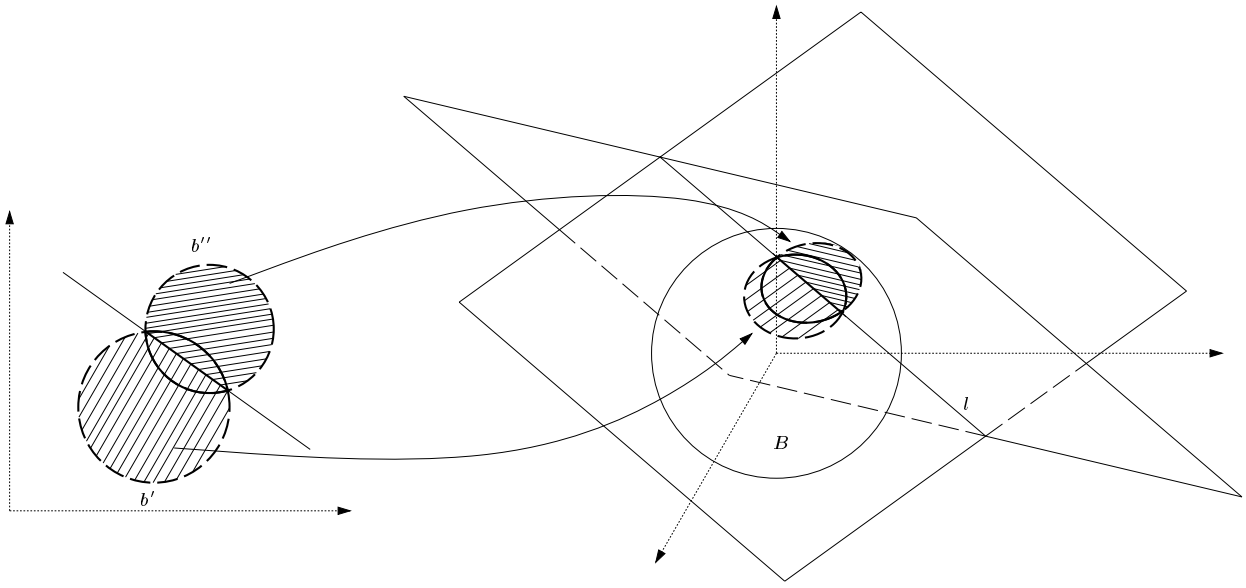

Figure 3: The intersection between the boundaries of two disks b', b'' in $\Re^2$ corresponds to a line l intersecting the sphere B.

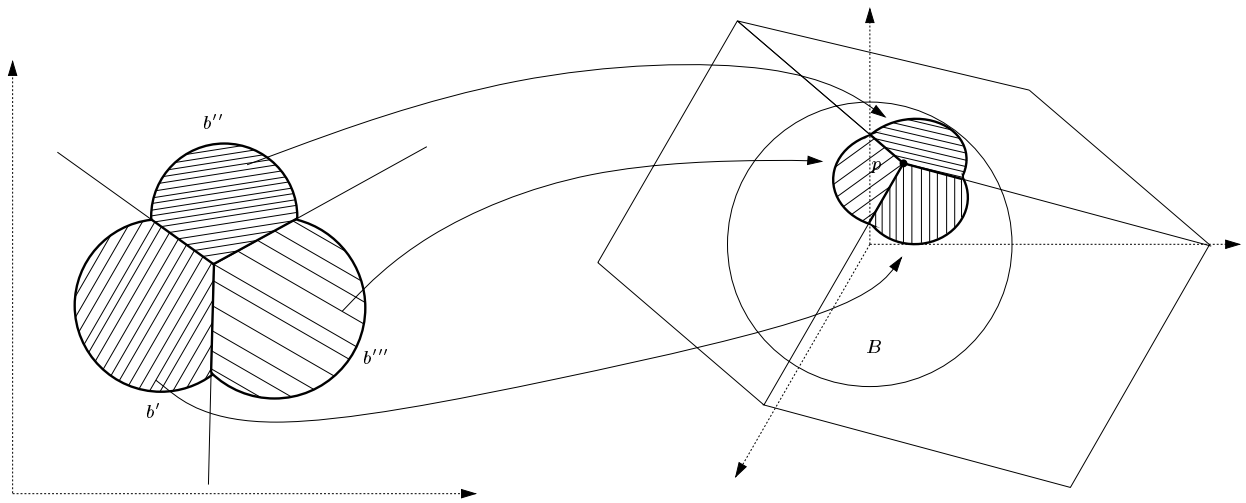

Figure 4: The non-empty intersection, when bounded by three circular arcs, between three disks b', b'', and b''' in $\Re^2$, corresponds to a point p contained in the ball B.

$$\dim\,(\partial b' \cap \partial b'' \cap \partial b''') = 0 \quad \Longleftrightarrow \quad p \in \partial B \ . \tag{9}$$

The proof of (8) is given in Appendix A.

This correspondence has a generalization to arbitrary dimensions. For dimension d, suppose we have $d+1$ balls $b^{(1)}$, ..., $b^{(d+1)}$ in $\Re^d$. Let $b^{(i)*}$ denote a region which can be either $b^{(i)}$ or its complement $\overline{b^{(i)}}$. Then if $b^{(1)*} \cap b^{(2)*} \cap \cdots \cap b^{(d+1)*} \neq \emptyset$ for all possible combinations of the $b^{(i)*}$, then the $d+1$ corresponding hyperplanes (of dimension d) intersect in a point contained in B.

Concentric spheres in $\Re^d$ generally correspond to hyperplanes in $\Re^{d+1}$ that pass through a specific hyperplane of dimension $d-1$. Explicitly, consider the set of spheres with center $(c_1, \cdots, c_d)$ and radii r_i. The corresponding hyperplanes are

$$(1 + c_1^2 + \cdots + c_d^2 - r_i^2) - 2(c_1\xi_1 + \cdots + c_d\xi_d) + (1 + c_1^2 + \cdots + c_d^2 + r_i^2)\xi_{d+1} = 0 \ .$$

These all contain the hyperplane of dimension $d-1$ defined by the intersection of $\xi_{d+1} = 1$ and $c_1\xi_1 + \cdots + c_d\xi_d = c_1^2 + \cdots + c_d^2 + 1$. There is an exceptional case when the common center of the spheres is the origin. In this case the corresponding hyperplanes are $1 - r_i^2 + (1 + r_i^2)\xi_{d+1} = 0$, or $\xi_{d+1} = (r_i^2 - 1)/(r_i^2 + 1)$, which form a set of hyperplanes parallel to and in between the hyperplanes $\xi_{d+1} = -1$ and $\xi_{d+1} = 1$.

Parallel hyperplanes in $\Re^{d+1}$ generally correspond to spheres with collinear centers in $\Re^d$. Explicitly, consider the set of hyperplanes $c_1\xi_1 + \cdots + c_{d+1}\xi_{d+1} = k_i$. In order that the corresponding spheres have real radii, we must have $k_i^2 \leq c_1^2 + \cdots c_{d+1}^2$. The corresponding spheres have centers $[-1/(c_{d+1} - k_i)](c_1, \ldots c_d)$ and radii $(c_1^2 + \cdots + c_{d+1}^2 - k_i^2)^{1/2}/|c_{d+1} - k_i|$. Thus the centers of these spheres all lie on the line through the origin in the direction $(c_1, \ldots, c_d)$. Furthermore, the intersections of these spheres with this line are such that the product of their distances to the point $[c_{d+1}/(c_1^2 + \cdots + c_d^2)](c_1, \ldots, c_d)$ is a constant, namely $(c_1^2 + \cdots + c_{d+1}^2)/(c_1^2 + \cdots + c_d^2)$. If one of the k_i should happen to equal c_{d+1}, then the corresponding sphere degenerates to a hyperplane of dimension $d-1$ through $[c_{d+1}/(c_1^2 + \cdots + c_d^2)](c_1, \ldots, c_d)$ and with normal vector $(c_1, \ldots, c_d)$. There is an exceptional case when the hyperplanes are parallel to $\xi_{d+1} = 0$, or equivalently, $c_1 = \cdots = c_d = 0$, $c_{d+1} \neq 0$. In this case the corresponding spheres are all centered at the origin, and have radii $(c_{d+1} - k_i)/(c_{d+1} + k_i)$. In order for the spheres to have positive radius, we need $|k_i| < |c_{d+1}|$. If $k_i = -c_{d+1}$, the sphere degenerates to a point, the origin, and if $k_i = c_{d+1}$, the corresponding sphere goes to infinity.

2.2 Convex Hulls and Boolean Combination of Balls

Consider the intersection of n balls or their complements, such as $b_1 \cap \bar{b}_2 \cap \bar{b}_3 \cap \cdots \cap b_n$. We can map each of the b_i or $\bar{b}_i$ to a halfspace h in $\Re^{d+1}$ so that the computation of the intersection is reduced to a convex hull computation. Note that if all the balls are complemented we get the complement of the union of balls as in [21]. In general, for the computation of the topological structure of a non-linear, non-convex, possibly disconnected region in $\Re^d$, the intersection of inequalities of the type (6) is reduced to the computation of the boundary of the convex polytope CP, intersection of halfspaces (4), and intersecting this boundary with the unit sphere (1).

This mapping generalizes the "lifting" scheme [18] so that it can represent both the interior and the exterior of balls and so that one can compute any boolean combination of balls instead of just their union. In the present formulation we also represent the balls by their implicit inequality (4) instead of just a center and a radius, so that one can deal with infinite radius spheres (note that such cases arise in practice in the computation of trimming curves).

An additional advantage of the present mapping with respect to the "lifting" scheme is the compact representation of several collections of curve arrangements in the special case of the collection of trimming circles of patches that form a molecular surface. In fact in this case we need only to observe that the convex polytope CP, that is dual to each arrangement of trimming curves of each patch, is indeed the cell of that patch in the 3-dimensional Power Diagram. This avoids the representation of a separate polytope CP per arrangement of trimming curves since the 3-dimensional Power Diagram contains all of them. The advantage in storage comes in representing only once any lower dimensional face sheared by more than one polytope and providing also, by this shearing of faces, explicit adjacency information for each boundary curve of each patch.

3 Maintaining Trimmed NURBS Under Quadratic Growth

We call quadratic growth the scheme of growing balls which keeps the Power Diagram unaltered and thus the topology of the union of balls is given by the corresponding α-shape. Under this growth of the balls we only need to maintain the set of trimming curves of each patch in the surface. In particular we need to efficiently detect any topological change (new intersections between curves, creation/deletion of connected components) that occur in the trimming curves (circles and lines) in the domain plane.

This goal can be achieved by looking at each patch separately (actually the computation can be

performed in parallel for all patches) and classifying the faces of its associated polytope CP with respect to the relative ball B at the current size. This is achieved by using the relations stated in Section 2.1 as follows:

- Each facet of CP that intersects ∂B corresponds to a circle that is effectively involved in the set of trimming curves.
- Each edge of CP that intersects ∂B corresponds to two circles that intersect each other.

This leads to the following algorithm for maintaining trimming curves. For each face f of CP we determine its minimum distance d_m and its maximum distance d_M from the origin (the center of B). This tells us when the circle associated with f is involved in the boundary of the trimming circles. We organize the ranges of all the faces in an Interval tree so that we can efficiently perform range queries, optimal in space and time. While growing the ball B we look at the faces of CP which range $[d_m, d_M]$ contains the current radius r of B to directly determine the topology of the trimming circles. For example, if the range of a facet of CP contains f but none of its boundary edges implies that an entire circle forms a separate component in the boundary of the trimming curves.

At the same time this tells us that in the growing process the values of d_m,d_M of the faces of CP constitute the set of "event points" at which the growth of r produces some topological change in the trimming circles. Hence we can efficiently maintain the dynamic arrangement of circles in the plane.

The topological structure of the molecule is given by the Regular Triangulation and its dual, the Power Diagram. We examine the family of triangulations that yield the topological structure of the molecular surfaces (solvent contact of solvent excluded surfaces) while the solvent radius grows.

The determination of the topological structure of such molecular surfaces is an important problem addressed by several papers [15, 16]. The family of shapes obtained from a weighted α-shape [19, 21, 22] is based on a quadratic growth of the radii of the balls and therefore not directly related to the family based on the growth of the solvent ball radius. In fact the fundamental property on which the α-shape construction is based on is that for any α, the Power Diagram/Regular Triangulation remains the same. This is achieved by growing each sphere by a different amount, namely the radius of each sphere is augmented by a quantity such that the square of each radius is increased by the same quantity (see figure 5). This implies that smaller spheres are grown more than the larger ones. As a consequence the resulting surface does not reflect exactly the required

molecular surface. When this level of approximation (possibly incorrect both in geometry and in topology) is not satisfactory, one needs to resort to the method introduced in the following section.

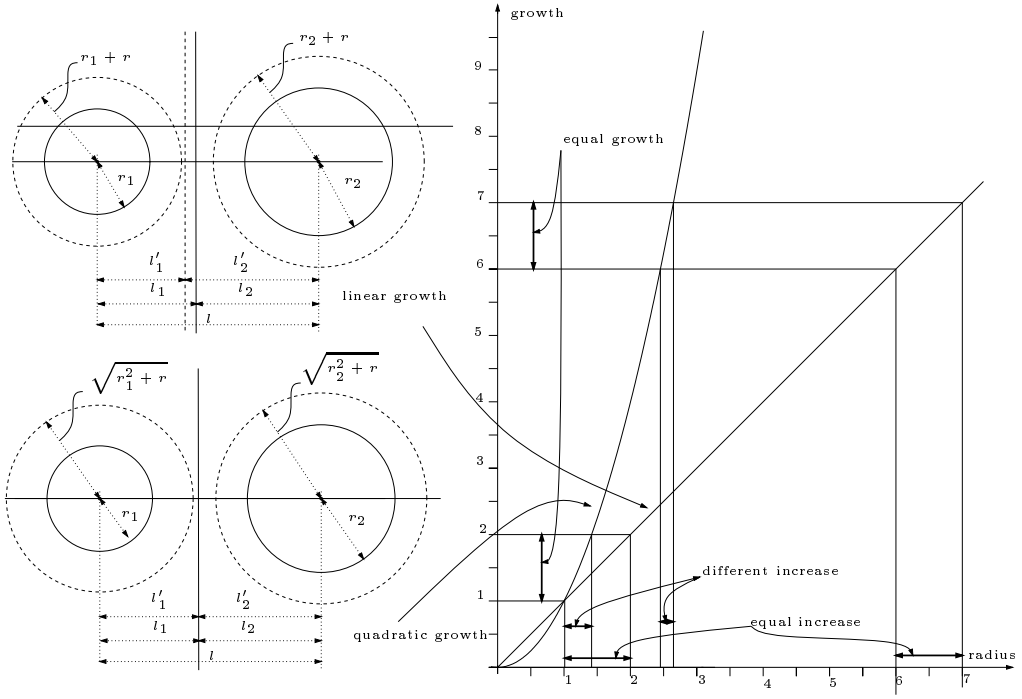

Figure 5: (a) If the radii of two balls are incremented by the same amount, then their Voronoi separator moves towards the smaller one. (b) If the squares of the radii of two balls are incremented by the same amount, then Voronoi separator remains the same.

4 Maintaining Trimmed NURBS under Linear Growth

The fundamental dynamic setting we consider is the case of a global linear growth of all the atoms of a molecule, corresponding to a linear growth of the solvent atom radius r. In this case the Voronoi Diagram (or more exactly Power Diagram) plane that separates the two balls moves as a function of r. In fact as the radius of each ball is increased by r, the Voronoi plane that separates the two balls moves towards the smaller ball. An example is shown in figure 5. The distances l_1, l_2 of the Voronoi plane π from the centers of the two balls must be such that the power distances of

π are equal, that is:

$$l_1^2 - r_1^2 = l_2^2 - r_2^2$$

Moreover, the distance between the two balls is constant (the two balls grow but do not move):

$$l_1 + l_2 = l$$

From these two equations we obtain for l_1:

$$l_1^2 - r_1^2 = (l - l_1)^2 - r_2^2 = l^2 + l_1^2 - 2l_1 l - r_2^2$$

$$l_1 = \frac{l^2 + r_1^2 - r_2^2}{2l}$$

When r_1 changes to $r_1 + r$ and r_2 changes to $r_2 + r$ we have:

$$\begin{aligned} l_1 &= \frac{l^2 + (r_1 + r)^2 - (r_2 + r)^2}{2l} \\ &= \frac{l^2 + r_1^2 + r^2 + 2r_1 r - r_2^2 - r^2 - 2r_2 r}{2l} \\ &= \frac{l^2 + r_1^2 - r_2^2 + 2r(r_1 - r_2)}{2l} \end{aligned}$$

In general, consider two balls B_1, B_2 (of radii r_1 and r_2 respectively) in $\Re^d$ and assume, without loss of generality, a coordinate system with the origin in the center of B_1 and the center of B_2 on the positive part of the x_1 axis (the center of B_2 is the point $(l, 0, \ldots, 0)$). The hyperplane of the Power Diagram that separates B_1 from B_2 has the equation:

$$\pi : \qquad x_1 = \frac{l^2 + r_1^2 - r_2^2}{2l} + r\frac{2(r_1 - r_2)}{2l} \tag{10}$$

which is linear in r. Hence this is also a hyperplane in the $(d+1)$-dimensional space $(x_1, \ldots, x_d, r)$. Figure 6 shows the 1-dimensional case of two balls (segments) that grow quadratically (a) or linearly (b). In the first case the hyperplane of the Power Diagram that separates B_1 from B_2 remains the same for all values of r. In the second case, the hyperplane of the Power Diagram that separates B_1 from B_2 moves linearly with r with a slope towards the center of B_1.

This fundamental observation leads to the construction of the Power Diagram of a set of growing balls as the intersection of a hyperplane $r = const$ with a complex $\mathcal{C}$ of convex polytopes in the $(d+1)$-dimensional space $(x_1, \ldots, x_d, r)$. If the molecule $\mathcal{B}$ is composed of n balls $\{B_1, \ldots, B_n\}$ then the complex $\mathcal{C}$ is a collection of n convex polytopes $\{C_1, \ldots, C_n\}$ one per ball. In particular the cell C_i associated with the ball B_i is the intersection of all the halfspaces of points "nearer" to B_i then to B_j (with $j = 1, \ldots, i-1, i+1, \ldots, n$). The boundary hyperplane of such halfspaces is given by

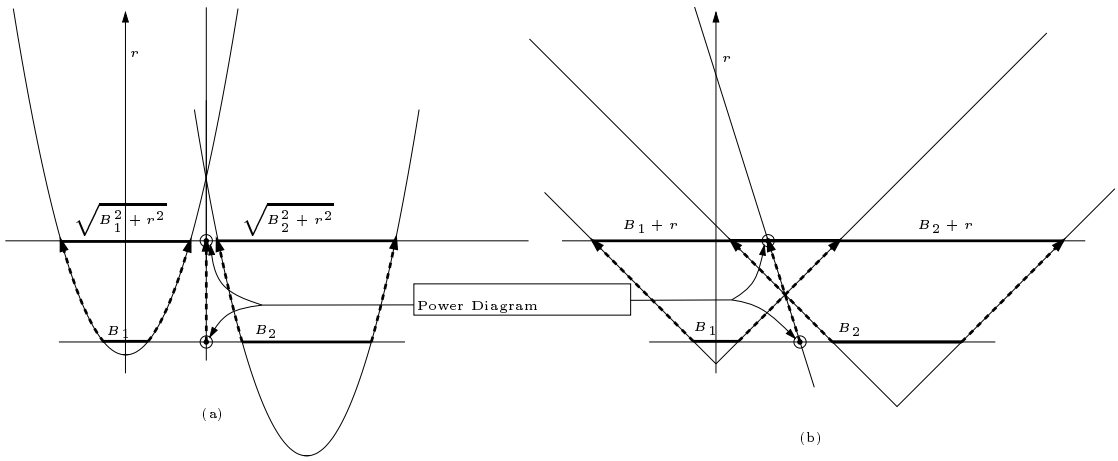

Figure 6: The 1-dimensional case of ball growth. The quadratic growth (a) keeps the Power Diagram hyperplane (a point) still. The linear growth (b) moves the Power Diagram hyperplane linearly with r.

equation (10). Note that cell C_i is defined as the intersection of all possible $n+1$ halfspaces since by linear growing many flips can occur in the Regular Triangulation. The brute force application of the technique as described here requires the computation of n convex hulls [10], which leads to an $O(n^3)$ time worst case complexity. For our purposes this is just a preprocessing step needed to construct the data-structure used for animating the molecular surface. So we do not report in the present paper the details of an efficient computation of this complex $\mathcal{C}$. Note however, that in the case of a molecule in three dimensions ($d = 3$) we have to compute a set of 4-dimensional convex hulls that can be computed more efficiently, in an output sensitive sense, by using the algorithm given in [9]. The use of this algorithm would indeed be beneficial because the overall number of faces in $\mathcal{C}$ is indeed $O(n^2)$. This is proved by a technique introduced in [7] that generalizes the "lifting" scheme for the computation of Power Diagrams [18] and maps the construction of the complex $\mathcal{C}$ to a convex hull computation (intersection of halfspaces) in one dimension higher (that is in dimension $d+2$). In the case of a molecule in the three dimensions, this leads to the computation of the convex hull in dimension five that can be computed optimally [10] in $O(n^2)$ time. This is certainly optimal in odd dimension (and in particular in the case of molecules where $d = 3$) since a single Power Diagram (and $\mathcal{C}$ contain many of them) already has the same number of faces as a $(d+1)$-dimensional convex polytope.

In the previous section we introduced the construction of a complex of convex polytopes $\mathcal{C}$

embedded in the $(d+1)$-dimensional space $(x_1, \ldots, x_d, r)$ whose "horizontal" slices (that is an intersection with the hyperplane $r = const$) are the Power Diagrams of the balls $\mathcal{B}$ with radii uniformly increased by r. This data-structure allows us to animate (update) efficiently the representation of a molecular surface (solvent accessible or solvent contact) with respect to a change in the solvent radius.

In particular we can achieve simple and efficient updates on the Power diagram localized in regions where the topological changes actually occur. In this way we can then in turn directly apply directly the method described in Section 3.

Being that the Power Diagram is the intersection of a horizontal hyperplane $H : r = const$ with the complex $\mathcal{C}$, in the dynamic setting the linear growth of the radii is simply a sweep of such horizontal hyperplanes H along the r-axis. Hence the "event points" at which we have to update the topological structure of the Power Diagram are the vertices of $\mathcal{C}$. In particular to compute these hyperplane sections of $\mathcal{C}$ we apply the robust approach in [6] which is based on the robust "above or "below" classification of the vertices of $\mathcal{C}$ with respect to H. We sort the vertices of $\mathcal{C}$ by their r coordinates so that their classification is obtained in logarithmic time by locating the current height value of H in such a sorted list of vertices. This approach is also suitable for the dynamic growth setting in which we will be continuously moving the hyperplane H. In fact in such a scenario, each time we cross a vertex of $\mathcal{C}$, we will need to update only the cells incident to this vertex. Moreover in general, if we suddenly change our solvent radius from a value r_1 to a value r_2, we will be able to detect the vertices whose r coordinate is in the range $[r_1, r_2]$, change their above/below classification and consequently update all the incident faces of $H \cap \mathcal{C}$.

We reach the conclusion that when spheres grow linearly, some flips can occur in the Regular Triangulation, unlike the quadratic growth, so that the usual α-shape construction is invalid (see figure 7).

5 Implementation Details and Examples

The first step in the implementation is a preprocessing step. We construct the complex C, and then let the hyperplane H sweep along the r-axis from $r = -\infty$ to $r = +\infty$ and record the flips [23] that occur dynamically. Second, once an array of flips sorted by r is obtained, make a logarithmic search of the initial value and perform the flips from that point up (or down) the destination r value. A compact representation of this algorithm is illustrated in Figure 8.

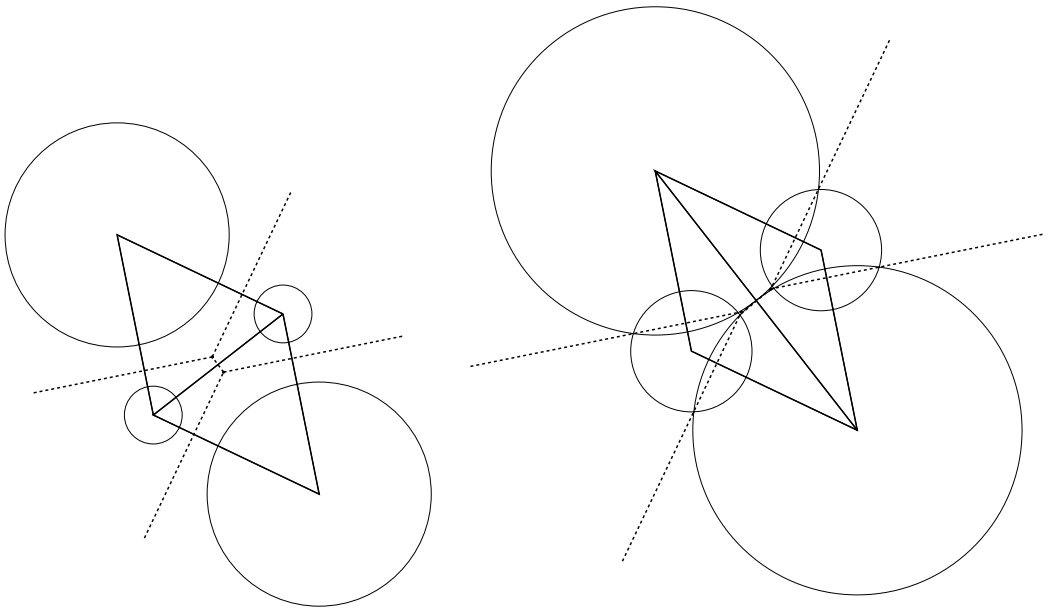

Figure 7: A simple case of a Regular Triangulation for which the topology changes in a simple linear growth of the radius of the balls.

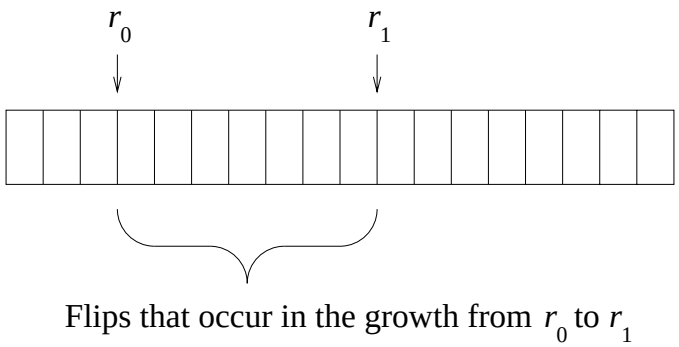

Figure 8: Flips in the Regular Triangulation as the radius r increases

Figure 9 illustrates an example of how the smoothed molecular surface changes as the radii of the atoms grow linearly. As the atoms grow, some of the interior balls are engulfed. Also the patches interpolating three atoms tend to consistently get wider.

In the following two subsections we provide detailed development of the method for two relatively simple cases. For a general setting we locally translate each atom to the origin of the reference system so that we can compute the trimming curves of the corresponding NURBS patch with the given expressions that are hence hardcoded in the program instead of being computed every time. To place the result in the global reference of the molecule we just need to apply the inverse mapping to the control points of the NURBS. The mapping is not applied to the trimming curves since they are defined in the parameter space of the NURBS patch.

5.1 Example 1

Here we choose a coordinate system so that two of the balls have centers on the ξ_1-axis in $\Re^3$. Specifically, consider three balls B', B'', and B'''. Choose a coordinate system so that their centers are located at $(0,0,0)$, $(l_{12},0,0)$, and $(l_{13}\cos\beta, l_{13}\sin\beta, 0)$, where l_{12} and l_{13} are the distances between the centers of B' and B'', and between the centers of B' and B''', respectively, and β is the angle made by the three centers, with B' at the vertex. We can assume $0 < \beta < \pi$. Let the solvent ball have radius r.

We consider the two planes π_1, π_2 relative to two trimming curves c_1, c_2. The position of the line $l = \pi_1 \cap \pi_2$ of intersection is used to track the intersection between c_1 and c_2 and to give their 2D NURBS representation.

With the above coordinate system, the two planes have equations (see figure 10):

$$\pi_1 \quad : \quad \xi_1 = a_1 + r a_2 \tag{11}$$

$$\pi_2 \quad : \quad (\cos\beta)\xi_1 + (\sin\beta)\xi_2 = a_3 + r a_4 \tag{12}$$

where

$$a_1 = \frac{l_{12}^2 + r_1^2 - r_2^2}{2l_{12}} \qquad a_2 = \frac{r_1 - r_2}{l_{12}}$$

$$a_3 = \frac{l_{13}^2 + r_1^2 - r_3^2}{2l_{13}} \qquad a_4 = \frac{r_1 - r_3}{l_{13}} \quad .$$

in accordance with (10).

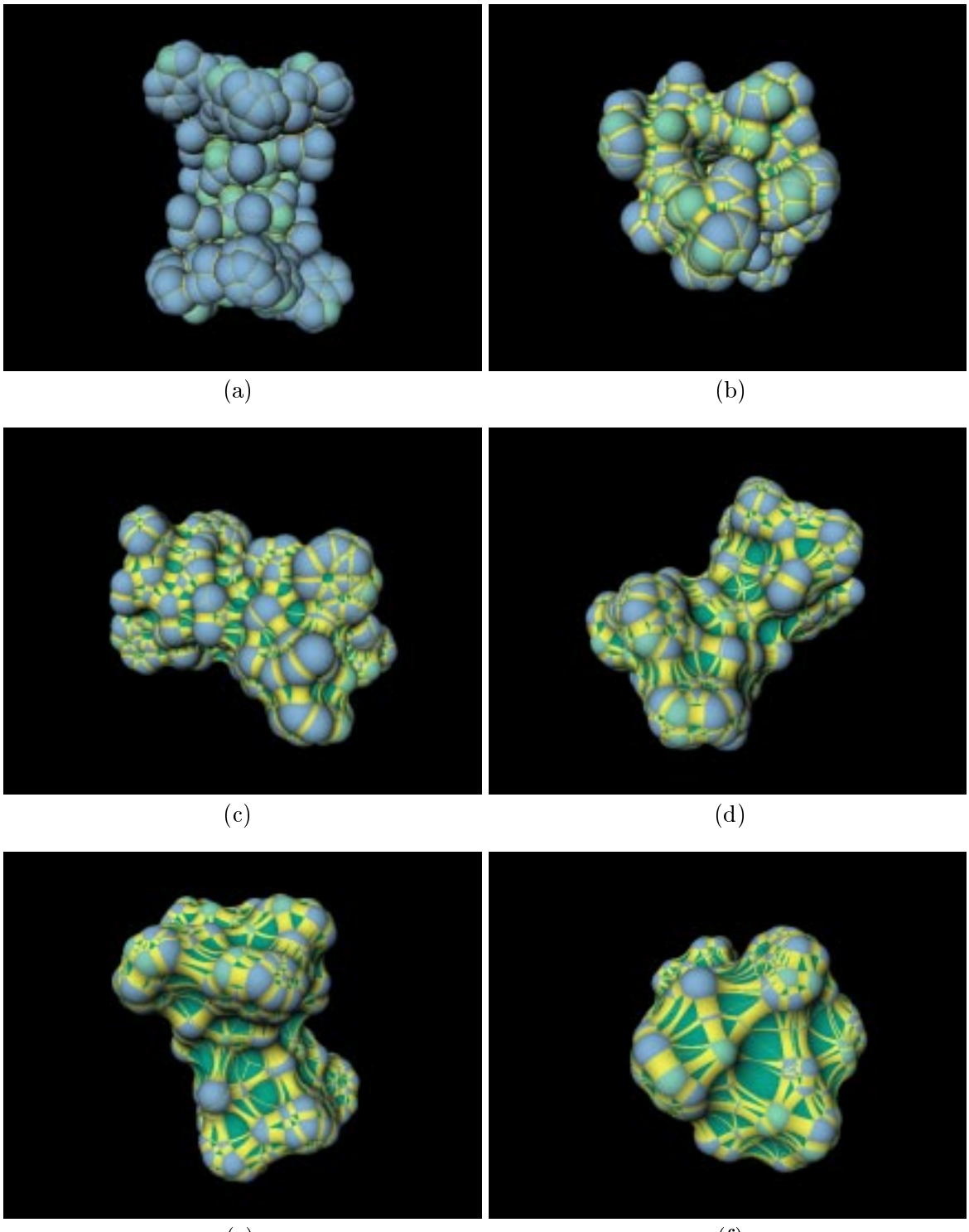

Figure 9: Molecular surface in which the radii of the atoms grow linearly at times (a) $t = 1$, (b) $t = 50$, (c) $t = 100$, (d) $t = 150$, (e) $t = 200$, (f) $t = 250$. The individual atoms are colored blue and cyan. Patches between two and three atoms are colored yellow and green, respectively. The topology of the union of patches changes over time.

The image of the trimming curve is the intersection of the spherical surfaces of the balls $B'(r)$ and $B''(r)$, which we define as the balls of radii $r_1 + r$ and $r_2 + r$ centered at $(0,0,0)$ and $(l_{12},0,0)$, respectively. The implicit equation of the spherical surface of $B'(r)$ is then $\xi_1^2 + \xi_2^2 + \xi_3^2 = (r_1 + r)^2$, and one find that the ξ_3 coordinate of the two points of intersection between this sphere and the line l is

$$\xi_3 \quad = \quad \pm\sqrt{(r_1 + r)^2 - \xi_1^2 - \xi_2^2} \tag{13}$$

The segment of the line $l = \pi_1 \cap \pi_2$ within $B'(r)$ then has the parametrization:

$$\begin{aligned} \xi_1 &= a_1 + r a_2 \\ \xi_2 &= a_5 + r a_6 \\ \xi_3 &= \sqrt{(r_1 + r)^2 - (a_1 + r a_2)^2 - (a_5 + r a_6)^2}\; u \quad , \end{aligned} \tag{14}$$

$$-1 \leq u \leq 1 \quad ,$$

where

$$a_5 = \frac{a_3 - a_1 \cos\beta}{\sin\beta} \qquad a_6 = \frac{a_4 - a_2 \cos\beta}{\sin\beta} \quad .$$

For brevity, these quantities which will appear frequently in the sequel will be named as follows. Keep in mind that all of these b_i are functions of r.

$$\begin{aligned} b_1 &= r_1 + r \\ b_2 &= a_1 + r a_2 \\ b_3 &= a_3 + r a_4 \\ b_4 &= a_5 + r a_6 \\ b_5 &= \sqrt{b_1^2 - b_2^2 - b_4^2} \\ b_6 &= \sqrt{b_1^2 - b_2^2} \\ b_7 &= \sqrt{b_2^2 + b_4^2} \end{aligned}$$

To map the surface of the ball $B'(r)$ to a plane, we use an inverse mapping similar to (3) but for a sphere of radius $r_1 + r$ instead of 1 and specifically $d = 2$:

$$\begin{aligned} x_1 &= \frac{\xi_1}{r_1 + r - \xi_3} \\ x_2 &= \frac{\xi_2}{r_1 + r - \xi_3} \quad . \end{aligned}$$

From this one obtains the intersection points q_1 and q_7 (see Figure 10(b); these points lie on a line through the origin) in the $(x_1(r), x_2(r))$ parameter space as

$$q_1 = \left(\frac{b_2}{b_1 + b_5}, \frac{b_4}{b_1 + b_5}\right)$$
$$q_7 = \left(\frac{b_2}{b_1 - b_5}, \frac{b_4}{b_1 - b_5}\right)$$

and the trimming curve is an arc of the circle with center

$$q_0 = \left(\frac{b_1}{b_2}, 0\right)$$

and radius

$$\frac{b_6}{b_2} \ .$$

One next needs to find suitable break points q_3 and q_5 (see Figure 10). Ideally we want none of the arcs $q_1\widehat{q_3}$, $q_3\widehat{q_5}$, $q_5\widehat{q_7}$ to be close to 180°. We can make sure that none of these arcs exceeds 120° as follows. Let q_8 be the midpoint of segment $\overline{q_1q_7}$, and let q_9 be the intersection of the perpendicular bisector of $\overline{q_1q_7}$ with the arc $q_3\widehat{q_5}$. Now choose q_3 and q_5 to be on the line perpendicular to $\overleftrightarrow{q_8q_9}$ that intersects the $\overleftrightarrow{q_8q_9}$ at a point 3/4 of the way from q_8 towards q_9. In the limiting case when q_1 and q_7 coincide, which occurs when $(r_1 + r)^2 = (a_1 + ra_2)^2 + (a_5 + ra_6)^2$, the three arcs $q_1\widehat{q_3}$, $q_3\widehat{q_5}$, $q_5\widehat{q_7}$ are all 120°, and they all shrink as the arc $q_1 - q_3 - q_5 - q_7$ shrinks.

In the x_1x_2-plane, line $\overleftrightarrow{q_1q_7}$ has the equation $(a_5 + ra_6)x - (a_1 + ra_2)y = 0$. We also have

$$q_8 = \left(\frac{b_1b_2}{b_7^2}, \frac{b_1b_4}{b_7^2}\right)$$

and

$$q_9 = \left(\frac{b_1}{b_2} + \frac{b_4b_6}{b_2b_7}, -\frac{b_6}{b_7}\right) \ .$$

From this we get

$$\begin{aligned} q_3 &= \left(\frac{4b_1b_7^2 - b_1b_4^2 + 3b_4b_6b_7}{4b_2b_7^2} - \frac{\sqrt{6b_1^2b_4^2 + 7b_2^2b_5^2 + 6b_1b_4b_6b_7}}{4b_7^2}, \right. \\ &\qquad \left. \frac{b_1b_4 - 3b_6b_7}{4b_7^2} - \frac{b_4\sqrt{6b_1^2b_4^2 + 7b_2^2b_5^2 + 6b_1b_4b_6b_7}}{4b_2b_7^2}\right) \\ q_5 &= \left(\frac{4b_1b_7^2 - b_1b_4^2 + 3b_4b_6b_7}{4b_2b_7^2} + \frac{\sqrt{6b_1^2b_4^2 + 7b_2^2b_5^2 + 6b_1b_4b_6b_7}}{4b_7^2}, \right. \\ &\qquad \left. \frac{b_1b_4 - 3b_6b_7}{4b_7^2} + \frac{b_4\sqrt{6b_1^2b_4^2 + 7b_2^2b_5^2 + 6b_1b_4b_6b_7}}{4b_2b_7^2}\right) \ . \end{aligned}$$

We now determine q_2, q_4, and q_6 as the points of intersection of the tangents lines through q_1, q_3, q_5, and q_7. We get

$$q_4 = \left(\frac{-7b_1^2b_4^3 + 4b_1^2b_4b_7^2 - 12b_1b_6b_7^3 - 7b_2^2b_4b_5^2 - 9b_4b_6^2b_7^2}{4b_2b_7^2(b_1b_4 - 3b_6b_7)}, \frac{7b_1^2b_4^2 + 7b_2^2b + 5^2 + 9b_6^2b_7^2}{4b_2b_7^2(b_1b_4 - 3b_6b_7)} \right) .$$

Also

$$\begin{aligned}
q_2 \;=\; & (1/d_1)\Big(b_2[7b_1^3b_2^2b_4^3 + 7b_1^3b_4^5 - 4b_1^3b_4^3b_7^2 + 7b_1^2b_2^2b_4^3b_5 + 4b_1^2b_2^2b_4b_5b_7^2 + 7b_1^2b_4^5b_5 \\
& - 4b_1^2b_4^3b_5b_7^2 + 12b_1^2b_4^2b_6b_7^3 + 7b_1b_2^4b_4b_5^2 + 7b_1b_2^2b_4^3b_5^2 - 4b_1b_2^2b_4^3b_7^2 + 13b_1b_2^2b_4b_6^2b_7^2 \\
& - 12b_1b_2^2b_5b_6b_7^3 + 9b_1b_4^3b_6^2b_7^2 + 12b_1b_4^2b_5b_6b_7^3 + 7b_2^4b_4b_5^3 + 7b_2^2b_4^3b_5^3 + 12b_2^2b_4^2b_6b_7^3 \\
& + 9b_2^2b_4b_5b_6^2b_7^2 - 12b_2^2b_6^3b_7^3 + 9b_4^3b_5b_6^2b_7^2 \\
& + (-4b_1^2b_2b_4b_7^2 - 8b_1b_2b_4b_5b_7^2 + 4b_2b_4^3b_7^2 - 4b_2b_4b_6^2b_7^2)c_1], \\
& 7b_1b_2^2b_4^2b_5^4 + 7b_1b_2^4b_5^2b_6^2 + 7b_1b_2^2b_4^2b_5^2b_6^2 + 7b_1^2b_2^2b_4^2b_5^3 + 7b_2^2b_4^2b_5^3b_6^2 + 12b_1^2b_4b_6^3b_7^3 \\
& + 9b_1b_4^2b_6^4b_7^2 + 7b_1^2b_2^2b_4^2b_5b_6^2 - 12b_2^2b_4b_6^3b_7^3 + 7b_1^3b_2^2b_4^2b_6^2 + 9b_1^2b_2^2b_5b_6^2b_7^2 - 12b_1b_2^2b_4b_5b_6b_7^3 \\
& - 4b_1b_2^2b_4^4b_7^2 + 7b_1^4b_2^2b_4^2b_5 - 4b_1^4b_4^2b_5b_7^2 + 4b_1^2b_2^2b_4^2b_5b_7^2 + 9b_1b_2^2b_6^4b_7^2 + 7b_1^2b_4^4b_5b_6^2 \\
& - 4b_1^3b_4^2b_6^2b_7^2 + 4b_1b_2^2b_4^2b_6^2b_7^2 - 4b_1^3b_4^2b_5^2b_7^2 + 9b_1b_2^2b_5^2b_6^2b_7^2 + 12b_1^2b_4b_5^2b_6b_7^3 + 9b_1b_4^2b_5^2b_6^2b_7^2 \\
& + 12b_1^3b_4b_5b_6b_7^3 + 7b_1^3b_2^2b_4^2b_5^2 + 5b_1^2b_4^2b_5b_6^2b_7^2 + 9b_2^2b_5b_6^4b_7^2 + 12b_1b_4b_5b_6^3b_7^3 + 9b_4^2b_5b_6^4b_7^2 \\
& + 7b_1^3b_4^4b_6^2 + 7b_1^4b_4^4b_5 + 7b_1^3b_4^4b_5^2 + 7b_1b_2^4b_5^3 + 7b_2^4b_5^3b_6^2 + 7b_1^2b_2^4b_5^3 + 12b_2^2b_4^3b_6b_7^3 \\
& + (-4b_1^3b_2b_5b_7^2 - 4b_1^2b_2b_5^2b_7^2 - 4b_1^2b_2b_6^2b_7^2 + 4b_1b_2^3b_5b_7^2 - 4b_1b_2b_5b_6^2b_7^2 - 4b_2^3b_4^2b_7^2 + 4b_2^3b_6^2b_7^2)c_1\Big)
\end{aligned}$$

and

$$\begin{aligned}
q_6 \;=\; & \frac{1}{d_2}\Big(b_2[4b_1^2b_4^3b_5b_7^2 - 9b_2^2b_4b_5b_6^2b_7^2 - 12b_1b_4^2b_5b_6b_7^3 - 9b_4^3b_5b_6^2b_7^2 + 7b_1^3b_5^4 + 12b_1^2b_4^2b_6b_7^3 \\
& + 9b_1b_4^3b_6^2b_7^2 - 7b_1^2b_2^2b_4^3b_5 + 12b_2^2b_4^2b_6b_7^3 - 12b_2^2b_6^3b_7^3 + 12b_1b_2^2b_5b_6b_7^3 - 4b_1^2b_2^2b_4b_5b_7^2 \\
& + 13b_1b_2^2b_4b_6^2b_7^2 + 7b_1^3b_2^2b_4^3 - 7b_1^2b_4^5b_5 - 4b_1^3b_4^3b_7^2 - 4b_1b_2^2b_4^3b_7^2 - 7b_2^4b_4b_5^3 \\
& - 7b_2^2b_4^3b_5^3 + 7b_1b_2^2b_4^3b_5^2 + 7b_1b_2^4b_4b_5^2 \\
& + (4b_1^2b_2b_4b_7^2 + 4b_2b_4b_6^2b_7^2 - 8b_1b_2b_4b_5b_7^2 - 4b_2b_4^3b_7^2)c_1], \\
& - 7b_1b_2^2b_4^2b_5^4 - 7b_1b_2^4b_5^2b_6^2 - 7b_1b_2^2b_4^2b_5^2b_6^2 + 7b_1^2b_2^2b_4^2b_5^3 + 7b_2^2b_4^2b_5^3b_6^2 - 12b_1^2b_4b_6^3b_7^3 \\
& - 9b_1b_4^2b_6^4b_7^2 + 7b_1^2b_2^2b_4^2b_5b_6^2 + 12b_2^2b_4b_6^3b_7^3 - 7b_1^3b_2^2b_4^2b_6^2 + 9b_1^2b_2^2b_5b_6^2b_7^2 - 12b_1b_2^2b_4b_5b_6b_7^3 \\
& + 4b_1b_2^2b_4^4b_7^2 + 7b_1^4b_2^2b_4^2b_5 - 4b_1^4b_4^2b_5b_7^2 + 4b_1^2b_2^2b_4^2b_5b_7^2 - 9b_1b_2^2b_6^4b_7^2 + 7b_1^2b_4^4b_5b_6^2 \\
& + 4b_1^3b_4^2b_6^2b_7^2 - 4b_1b_2^2b_4^2b_6^2b_7^2 + 4b_1^3b_4^2b_5^2b_7^2 - 9b_1b_2^2b_5^2b_6^2b_7^2 - 12b_1^2b_4b_5^2b_6b_7^3 - 9b_1b_4^2b_5^2b_6^2b_7^2 \\
& + 12b_1^3b_4b_5b_6b_7^3 - 7b_1^3b_2^2b_4^2b_5^2 + 5b_1^2b_4^2b_5b_6^2b_7^2 + 9b_2^2b_5b_6^4b_7^2 + 12b_1b_4b_5b_6^3b_7^3 + 9b_4^2b_5b_6^4b_7^2
\end{aligned}$$

$$- 7b_1^3b_4^4b_6^2 + 7b_1^4b_4^4b_5 - 7b_1^3b_4^4b_5^2 - 7b_1b_2^4b_5^4 + 7b_2^4b_5^3b_6^2 + 7b_1^2b_2^4b_5^3 - 12b_2^2b_4^3b_6b_7^3$$
$$+(4b_2^3b_6^2b_7^2 - 4b_1^2b_2b_5^2b_7^2 + 4b_1b_2b_5b_6^2b_7^2 + 4b_1^3b_2b_5b_7^2 - 4b_1^2b_2b_6^2b_7^2 - 4b_1b_2^3b_5b_7^2 - 4b_2^3b_4^2b_7^2)c_1\Big)$$

where

$$\begin{aligned}
c_1 &= \sqrt{6b_1^2b_4^2 + 7b_2^2b_5^2 + 6b_1b_4b_6b_7} \\
d_1 &= b_7^2(b_1+b_5)[(-b_1b_4b_5 - b_2^2b_4 - b_4b_6^2)c_1 \\
&\quad + b_1^2b_2b_4b_5 - b_1b_2b_4^3 + b_1b_2b_4b_6^2 - 3b_1b_2b_5b_6b_7 + 3b_2b_4^2b_6b_7 - 3b_2b_6^3b_7] \\
d_2 &= b_7^2(b_1-b_5)[(b_1b_4b_5 - b_2^2b_4 - b_4b_6^2)c_1 \\
&\quad + b_1^2b_2b_4b_5 + b_1b_2b_4^3 - b_1b_2b_4b_6^2 - 3b_1b_2b_5b_6b_7 - 3b_2b_4^2b_6b_7 + 3b_2b_6^3b_7]
\end{aligned}$$

We now need rational parametrizations of the circular arcs. The parametrization for arc $q_1 - q_2 - q_3$ is provided by

$$(x_1, x_2) = \frac{(1-t)^2q_3 + 2t(1-t)w_1q_2 + t^2q_1}{(1-t)^2 + 2t(1-t)w_1 + t^2} \quad , \quad 0 \le t \le 1 \, ,$$

for a particular value for the weight w_1, which turns out to be the cosine of half the angle $\angle q_1q_0q_3$, or $\cos q_1q_0q_2$. This can be computed as

$$w_1 = \frac{(q_1 - q_0)\cdot(q_2 - q_0)}{\|q_1 - q_0\|\|q_2 - q_0\|} \quad .$$

Analogous parametrizations hold for arcs $q_3 - q_4 - q_5$ and $q_5 - q_6 - q_7$.

5.2 Example 2

Here we place the balls in $\Re^3$ so that the line through the endpoints of a trimming arc is parallel to the x_1-axis in x_1x_2-space. Consider three balls B', B'', and B'''. Choose a coordinate system so that their centers are located at $(0,0,0)$, $(l_{12}\cos\alpha, -l_{12}\sin\alpha, 0)$, and $(l_{13}\cos(\beta-\alpha), l_{13}\sin(\beta-\alpha), 0)$ where l_{12} and l_{13} are the distances between the centers of B' and B'', and between the centers of B' and B''', respectively, β is the angle made by the three centers, with B' at the vertex $(0 < \beta < \pi)$, and

$$\alpha = \tan^{-1}\left[\frac{(a_3 + ra_4) - (a_1 + ra_2)\cos\beta}{(a_1 + ra_2)\sin\beta}\right] \quad .$$

With this definition we have that α is the angle between the ray through the centers of B' and B'', and the ξ_1-axis, and

$$\begin{aligned}
\cos\alpha &= \frac{b_2\sin\beta}{(b_2^2 - 2b_2b_3\cos\beta + b_3^2)^{1/2}} \\
\sin\alpha &= \frac{b_3 - b_2\cos\beta}{(b_2^2 - 2b_2b_3\cos\beta + b_3^2)^{1/2}} \quad .
\end{aligned}$$

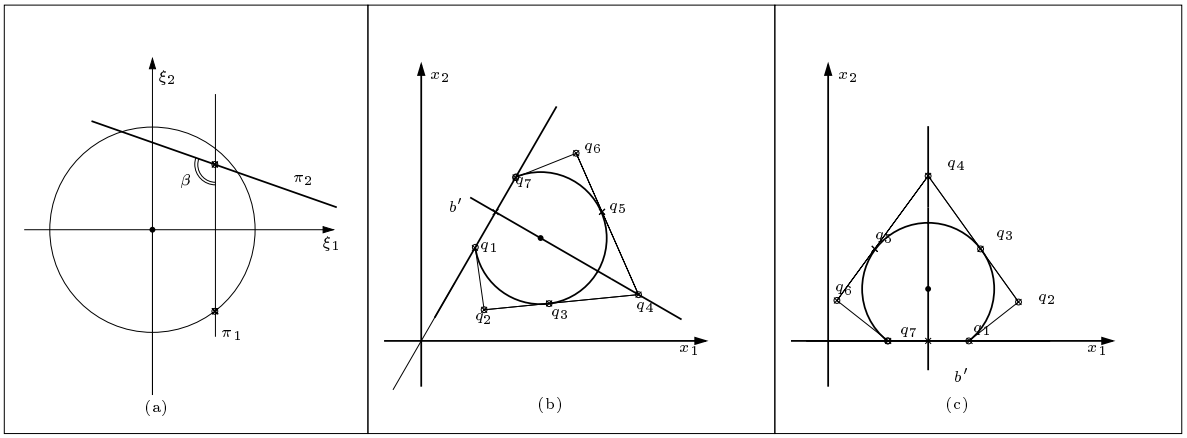

Figure 10: (a) (ξ_1, ξ_2) section of the (ξ_1, ξ_2, ξ_3) space. The circle is a cross section of ball $B'(r)$ of radius $r_1 + r$. Line l, which is parallel to the ξ_3 axis, is the intersection of the planes π_1 and π_2, which in turn are the Voronoi planes separating $B'(r)$ and $B''(r)$ and separating $B'(r)$ and $B'''(r)$. (b) control points of the trimming curve that is part of the boundary of $b'(r)$ for Example 1. (c) the same control points in Example 2.

Note that α is a function of r. This coordinate system is chosen so that the Voronoi planes defined below intersect at the ξ_1-axis.

Let the solvent ball have radius r. We consider the two planes π_1, π_2 relative to two trimming curves c_1, c_2. The position of the line $l = \pi_1 \cap \pi_2$ of intersection is used to track the intersection between c_1 and c_2 and to give their 2D NURBS representation.

With the above coordinate system, the two planes have equations:

$$\pi_1 \quad : \quad (\cos\alpha)\xi_1 - (\sin\alpha)\xi_2 = a_1 + ra_2 \tag{15}$$

$$\pi_2 \quad : \quad [\cos(\beta - \alpha)]\xi_1 + [\sin(\beta - \alpha)]\xi_2 = a_3 + ra_4 \tag{16}$$

where

$$a_1 = \frac{l_{12}^2 + r_1^2 - r_2^2}{2l_{12}} \qquad a_2 = \frac{r_1 - r_2}{l_{12}}$$

$$a_3 = \frac{l_{13}^2 + r_1^2 - r_3^2}{2l_{13}} \qquad a_4 = \frac{r_1 - r_3}{l_{13}} \quad .$$

in accordance with (10).

The image of the trimming curve is the intersection of the spherical surfaces of the balls $B'(r)$ and $B''(r)$, which we define as the balls of radii $r_1 + r$ and $r_2 + r$ centered at $(0, 0, 0)$

and $(l_{12}\cos\alpha, -l_{12}\sin\alpha, 0)$, respectively. The implicit equation of the spherical surface of $B'(r)$ is then $\xi_1^2 + \xi_2^2 + \xi_3^2 = (r_1 + r)^2$, and one find that the ξ_3 coordinate of the two points of intersection between this sphere and the line l is

$$\xi_3 \;=\; \pm\sqrt{(r_1+r)^2 - \xi_1^2 - \xi_2^2} \tag{17}$$

The segment of the line $l = \pi_1 \cap \pi_2$ within $B'(r)$ then has the parametrization:

$$\begin{aligned} \xi_1 &= (a_1 + ra_2)/\cos\alpha \\ \xi_2 &= 0 \\ \xi_3 &= \sqrt{(r_1+r)^2 - (a_1+ra_2)^2/\cos^2\alpha}\; u \quad , \end{aligned} \tag{18}$$

$$-1 \le u \le 1 \quad .$$

To map the surface of the ball $B'(r)$ to a plane, we use an inverse mapping similar to (3) but for a sphere of radius $r_1 + r$ instead of 1 and specifically $d = 2$:

$$\begin{aligned} x_1 &= \frac{\xi_1}{r_1 + r - \xi_3} \\ x_2 &= \frac{\xi_2}{r_1 + r - \xi_3} \quad . \end{aligned}$$

From this one obtains the intersection points q_1 and q_7 (see Figure 10(c)) in the $(x_1(r), x_2(r))$ parameter space as

$$q_1 = \left(\frac{b_1\cos\alpha - \sqrt{b_1^2\cos^2\alpha - b_2^2}}{b_2}, 0 \right)$$
$$q_7 = \left(\frac{b_1\cos\alpha + \sqrt{b_1^2\cos^2\alpha - b_2^2}}{b_2}, 0 \right)$$

and the trimming curve is an arc of the circle with center

$$q_0 = \left(\frac{b_1\cos\alpha}{b_2}, -\frac{b_1\sin\alpha}{b_2} \right)$$

and radius

$$\frac{b_6}{b_2} \quad .$$

In the x_1x_2-plane, line $\overleftrightarrow{q_1q_7}$ is just the x_1-axis, and line $\overleftrightarrow{q_8q_9}$ is $x_1 = b_1\cos\alpha/b_2$. We also have

$$q_8 = \left(\frac{b_1\cos\alpha}{b_2}, 0 \right)$$

and

$$q_9 = \left(\frac{b_1\cos\alpha}{b_2}, -\frac{b_1\sin\alpha + b_6}{b_2} \right) \quad .$$

From this we find that the break points q_3 and q_5 are

$$\begin{aligned} q_3 &= \left(\frac{b_1 \cos\alpha}{b_2} - \frac{(7b_6^2 - b_1^2 \sin^2\alpha + 6b_1 b_6 \sin\alpha)^{1/2}}{4b_2}, -\frac{3}{4}\frac{b_1 \sin\alpha + b_6}{b_2} \right) \\ q_5 &= \left(\frac{b_1 \cos\alpha}{b_2} + \frac{(7b_6^2 - b_1^2 \sin^2\alpha + 6b_1 b_6 \sin\alpha)^{1/2}}{4b_2}, -\frac{3}{4}\frac{b_1 \sin\alpha + b_6}{b_2} \right) \quad . \end{aligned}$$

We now determine q_2, q_4, and q_6 as the points of intersection of the tangents lines through q_1, q_3, q_5, and q_7. We get

$$q_4 = \left(\frac{b_1 \cos\alpha}{b_2}, -\frac{b_1 \sin\alpha}{b_2} + \frac{4b_6^2}{b_2(b_1 \sin\alpha - 3b_6)} \right) \quad .$$

Also

$$q_2 = \left(\frac{b_1 \cos\alpha}{b_2} - \frac{3b_6^2(b_1 \sin\alpha + b_6)}{b_2[b_1(c_2 - c_1)\sin\alpha + 3b_6 c_1]}, -\frac{b_1 \sin\alpha}{b_2} + \frac{b_6^2(c_2 - 4c_1)}{b_2[b_1(c_2 - c_1)\sin\alpha + 3b_6 c_1]} \right)$$

and

$$q_6 = \left(\frac{b_1 \cos\alpha}{b_2} + \frac{3b_6^2(b_1 \sin\alpha + b_6)}{b_2[b_1(c_2 - c_1)\sin\alpha + 3b_6 c_1]}, -\frac{b_1 \sin\alpha}{b_2} + \frac{b_6^2(c_2 - 4c_1)}{b_2[b_1(c_2 - c_1)\sin\alpha + 3b_6 c_1]} \right)$$

where

$$\begin{aligned} c_1 &= \sqrt{b_1^2 \cos^2\alpha - b_2^2} \\ c_2 &= \sqrt{7b_6^2 - b_1^2 \sin^2\alpha + 6b_1 b_6 \sin\alpha} \quad . \end{aligned}$$

6 Conclusions

We have described modeling and animation algorithms that dynamically update and render exact and smoothed molecular surface representations for moving or growing collections of balls. Two main classes were considered: one where the radii of the atoms grow quadratically so that the Power Diagram remains fixed, and the other in which the atom radii grow linearly and the Power Diagram is updated continuously. In the first case accuracy of the solution is sacrificed for speed of the computation to allow fast user interaction times. In the latter case the exact solution is given at a higher computation cost for the case where higher accuracy is needed. The use of these algorithms can enable one to manipulate molecular models and smoothed molecular surfaces in a wide variety of applications.

Appendix A: Proof of equation (8)

Let the three circles be $(x-x_i)^2+(y-y_i)^2=r_i^2$, $i=1,2,3$. Then the three corresponding planes are $(1+x_i^2+y_i^2-r_i^2)-2x_i\xi_1-2y_i\xi_2+(1-x_i^2-y_i^2+r_i^2)\xi_3=0$. Their point of intersection, if unique and finite, is given by $(\xi_1,\xi_2,\xi_3)=(D_1/D_4, D_2/D_4, D_3/D_4)$, where

$$D_1=\begin{vmatrix} -1-x_1^2-y_1^2+r_1^2 & -2y_1 & 1-x_1^2-y_1^2+r_1^2 \\ -1-x_2^2-y_2^2+r_2^2 & -2y_2 & 1-x_2^2-y_2^2+r_2^2 \\ -1-x_3^2-y_3^2+r_3^2 & -2y_3 & 1-x_3^2-y_3^2+r_3^2 \end{vmatrix},$$

$$D_2=\begin{vmatrix} -2x_1 & -1-x_1^2-y_1^2+r_1^2 & 1-x_1^2-y_1^2+r_1^2 \\ -2x_2 & -1-x_2^2-y_2^2+r_2^2 & 1-x_2^2-y_2^2+r_2^2 \\ -2x_3 & -1-x_3^2-y_3^2+r_3^2 & 1-x_3^2-y_3^2+r_3^2 \end{vmatrix},$$

$$D_3=\begin{vmatrix} -2x_1 & -2y_1 & -1-x_1^2-y_1^2+r_1^2 \\ -2x_2 & -2y_2 & -1-x_2^2-y_2^2+r_2^2 \\ -2x_3 & -2y_3 & -1-x_3^2-y_3^2+r_3^2 \end{vmatrix}, \quad D_4=\begin{vmatrix} -2x_1 & -2y_1 & 1-x_1^2-y_1^2+r_1^2 \\ -2x_2 & -2y_2 & 1-x_2^2-y_2^2+r_2^2 \\ -2x_3 & -2y_3 & 1-x_3^2-y_3^2+r_3^2 \end{vmatrix}.$$

The condition that this point of intersection lies in the interior of B is

$$D_1^2+D_2^2+D_3^2-D_4^2<0 \ . \tag{19}$$

If $D_4=0$, then the point of intersection is at infinity, and the inequality (19) cannot be satisfied. (If $D_1=D_2=D_3=D_4=0$, then the three planes have a line in common which intersects B, and it can be shown that the centers of the three circles are collinear and the circles intersect in two points.)

The intersection of three disks is bounded by three circular arcs exactly when each disk contains exactly one of the two points of intersection of the other two circles. In order for the first two circles to intersect in two points, we need that the distance between their centers is strictly between $|r_1-r+2|$ and r_1+r_2. This can be expressed algebraically as

$$A_1=[(x_1-x_2)^2+(y_1-y_2)^2-(r_1-r_2)^2][(x_1-x_2)^2+(y_1-y_2)^2-(r_1+r_2)^2]<0 \ . \tag{20}$$

Next, we need that r_3 is between the distance from (x_3,y_3) to the two points of intersection of the first two circles. This condition turns out to be expressible as

$$\frac{\begin{vmatrix} x_1 & x_2 & x_3 \\ y_1 & y_2 & y_3 \\ 1 & 1 & 1 \end{vmatrix}^2 A_1+A_2^2}{[(x_1-x_2)^2+(y_1-y_2)^2]^2}<0 \tag{21}$$

where

$$\begin{aligned} A_2 &= [(x_2-x_1)(x_2-x_3)+(y_2-y_1)(y_2-y_3)]r_1^2 \\ &\quad + [(x_2-x_1)(x_3-x_1)+(y_2-y_1)(y_3-y_1)]r_2^2 \\ &\quad + [(x_2-x_1)^2+(y_2-y_1)^2][(x_3-x_1)(x_3-x_2)+(y_3-y_1)(y_3-y_2)-r_3^2] \ . \end{aligned}$$

Remarkably,

$$D_1^2+D_2^2+D_3^2-D_4^2 = \begin{vmatrix} x_1 & x_2 & x_3 \\ y_1 & y_2 & y_3 \\ 1 & 1 & 1 \end{vmatrix}^2 A_1+A_2^2 \ .$$

Therefore, if the intersection of the three disks is bounded by three circular arcs ((20) and (21) hold), then the intersection point of the three planes is within B ((19) holds). If the intersection point of the three planes is a point within B ((19) holds), then (21) holds. Since (21) holds, we must have $A_1 < 0$, so that (20) holds as well, and then the three circles intersect pairwise in two points, and each disk contains exactly one of the two points of intersection of the other two circles.

References

[1] N. Akkiraju and H. Edelsbrunner. Triangulating the surface of a molecule. *Discrete Applied Mathematics*, 71:5–22, 1996.

[2] G. Albers and T. Roos. Voronoi diagrams of moving points in higher dimensional spaces. In *Proc. 3rd Scand. Workshop Algorithm Theory*, volume 621 of *Lecture Notes in Computer Science*, pages 399–409. Springer-Verlag, 1992.

[3] F. Aurenhammer. Power diagrams: Properties, algorithms, and applications. *SIAM Journal of Computing*, 16(1):78–96, 1987.

[4] C. L. Bajaj and W. J. Bouma. Dynamic Voronoi diagrams and Delaunay triangulations. In *Proc. 2nd Canadian Conference on Computational Geometry*, pages 273–277, 1990.

[5] C. L. Bajaj, H. Y. Lee, R. Merkert, and V. Pascucci. NURBS based B-rep models for macromolecules and their properties. In *Proceedings of the 4th Symposium on Solid Modeling and Applications*, pages 217–228, New York, May 1997. ACM Press.

[6] C. L. Bajaj and V. Pascucci. Splitting a complex of convex polytopes in any dimension. In *Proceedings of the Twelfth Annual Symposium On Computational Geometry (ISG '96)*, pages 88–97, New York, May 1996. ACM Press.

[7] C. L. Bajaj and V. Pascucci. Wrapping the Voronoi diagram: A constructive approach to duality. Technical report, University of Texas, Austin, TX 78712, 1997.

[8] James F. Blinn. A generalization of algebraic surface drawing. *ACM Transactions on Graphics*, 1(3):235–256, July 1982.

[9] T. M. Y. Chan, J. Snoeyink, and C.-K. Yap. Output-sensitive construction of polytopes in four dimensions and clipped Voronoi diagrams in three. In *Proceedings of the Sixth Annual ACM-SIAM Symposium on Discrete Algorithms*, pages 282–291, San Francisco, California, January 1995.

[10] B. Chazelle. An optimal convex hull algorithm in any fixed dimension. *Discrete & Computational Geometry*, 10:377–409, 1993.

[11] P. Chew. Near-quadratic bounds for the L_1 Voronoi diagram of moving points. *Computational Geometry Theory and Applications*, 7, 1997.

[12] M. L. Connolly. Analytical molecular surface calculation. *Journal of Applied Crystallography*, 16:548–558, 1983.

[13] M. L. Connolly. Solvent-accessible surfaces of proteins and nucleic acids. *Science*, 221:709–713, 1983.

[14] M. L. Connolly, T.J. O'Donnell, and S. Warde. Special issue on molecular surfaces. *Network Science*, 2(4), April 1996. M. L. Connolly "Molecular Surfaces: A Review", T.J. O'Donnell "The Scientific and Artistic Uses of Molecular Surfaces", S. Warde "Molecular Modeling and Simulation of Surfaces," http://edisto.awod.com/netsci/Issues/1996/Apr/articles.html.

[15] C. J. A. Delfinado and H. Edelsbrunner. An incremental algorithm for Betti numbers of simplicial complexes. In *Proc. 9th Annual ACM Symposium on Computational Geometry*, pages 232–239, 1993.

[16] C. J. A. Delfinado and H. Edelsbrunner. An incremental algorithm for Betti numbers of simplicial complexes on the 3-sphere. *Computer Aided Geometric Design*, 12(7):771–784, 1995. Grid generation, finite elements, and geometric design.

[17] Mathieu Desbrun and Marie-Paule Gascuel. Animating soft substances with implicit surfaces. In Robert Cook, editor, *SIGGRAPH 95 Conference Proceedings*, Annual Conference Series, pages 287–290. ACM SIGGRAPH, Addison Wesley, August 1995. held in Los Angeles, California, 06-11 August 1995.

[18] H. Edelsbrunner. *Algorithms in Combinatorial Geometry*, volume 10 of *EATCS Monographs on Theoretical Computer Science*. Springer-Verlag, Heidelberg, West Germany, 1987.

[19] H. Edelsbrunner. Weighted alpha shapes. Technical Report 1760, University of Illinois at Urbana-Champaign, 1992.

[20] H. Edelsbrunner. Smooth surfaces for multi-scale shape representation. In *Proc. 15th Conf. Found. Softw. Tech. Theoret. Comput. Sci.*, volume 1026 of *Lecture Notes in Computer Science*, pages 391–412. Springer-Verlag, 1995.

[21] H. Edelsbrunner. The union of balls and its dual shape. *Discrete & Computational Geometry*, 13(3-4):415–440, 1995.

[22] H. Edelsbrunner and E. P. Mücke. Three-dimensional alpha shapes. *ACM Transactions on Graphics*, 13(1):43–72, January 1994.

[23] H. Edelsbrunner and N. R. Shah. Incremental topological flipping works for regular triangulations. *Algorithmica*, 15:223–241, 1996.

[24] M. A. Facello. *Geometric Techniques for Molecular Shape Analysis*. PhD thesis, University of Illinois, 1996. Department of Computer Science Technical Report # 1967.

[25] J. J. Fu and R. C. T. Lee. Voronoi diagrams of moving points in the plane. *International Journal of Computational Geometry and Applications*, 1(1):23–32, 1991.

[26] Takushi Fujita, Katsuhiko Hirota, and Kouichi Murakami. Representation of splashing water using metaball model. *Fujitsu*, 41(2):159–165, 1990. in Japanese.

[27] G. Graves. The magic of metaballs. *Computer Graphics World*, 16(5):27–32, 1993.

[28] L. Guibas, J. S. B. Mitchell, and T. Roos. Voronoi diagrams of moving points in the plane. In *Proc. 17th Internat. Workshop Graph-Theoret. Concepts Comput. Sci.*, volume 570 of *Lecture Notes in Computer Science*, pages 113–125. Springer-Verlag, 1991.

[29] P. M. Hubbard. Approximating polyhedra with spheres for time-critical collision detection. *ACM Transactions on Graphics*, 15(3), 1996.

[30] H. Imai, M. Iri, and K. Murota. Voronoi diagram in the laguerre geometry and its applications. *SIAM Journal of Computing*, 14:93–10, 1985.

[31] S. Krishnan, D. Manocha, and A. Narkhede. Representation and evaluation of boolean combinations of NURBS solids. In *Fifth MSI-Stony Brook Workshop on Computational Geometry, Stony Brook*, October 1995.

[32] S. Kumar, D. Manocha, and A. Lastra. Interactive display of large-scale NURBS models. *IEEE Transactions on Visualization and Computer Graphics*, 2(4):323–336, 1996.

[33] N. L. Max. Computer representation of molecular surfaces. *IEEE Computer Graphics and Applications*, 3(5):21–29, August 1983.

[34] H. Nishimura, M. Hirai, T. Kawai, T. Kawata, I. Shirakawa, and K. Omura. Object modeling by distribution function and a method of image generation. *Transactions IECE Japan, Part D*, J68-D(4):718–725, 1985.

[35] T. Nishita and E. Nakamae. A method for displaying metaballs by using Bézier clipping. In *Computer Graphics Forum*, volume 13, pages 271–280. Eurographics, Basil Blackwell Ltd, 1994. Eurographics '94 Conference issue.

[36] T. Roos. Voronoĭ diagrams over dynamic scenes. *Discrete Applied Mathematics. Combinatorial Algorithms, Optimization and Computer Science*, 43(3):243–259, 1993.

[37] T. Roos. New upper bounds on Voronoi diagrams of moving points. *Nordic Journal of Computing*, 4(2):167–171, 1997.

[38] M. F. Sanner and A. J. Olson. Reduced surface: An efficient way to compute molecule surfaces. *Biopolymers*, 38:305–320, 1996.

[39] M. F. Sanner and A. J. Olson. Real time surface reconstruction for moving molecular fragments. In *Proc. of Pacific Symposium on Biocomputing '97*, Maui, Hawaii, January 1997.

[40] M. F. Sanner, A. J. Olson, and J. C. Spehner. Fast and robust computation of molecular surfaces. In *Proc. 11th Annual ACM Symposium on Computational Geometry*, pages C6–C7, 1995.

[41] D. Terzopoulos and H. Qin. Dynamic NURBS with geometric constraints for interactive sculpting. *ACM Transactions on Graphics*, 13(2):103–136, 1994.

[42] A. Varshney and F. P. Brooks, Jr. Fast analytical computation of Richard's smooth molecular surface. In Gregory M. Nielson and Dan Bergeron, editors, *Proceedings of the Visualization '93 Conference*, pages 300–307, San Jose, CA, October 1993. IEEE Computer Society Press.

[43] R. Voorintholt, M. T. Kosters, and G. Vegter. A very fast program for visualizing protein surfaces, channels and cavities. *Journal on Molecular Graphics*, 7:243–245, December 1989.

[44] J. Wernecke. *The Inventor Mentor*. Addison–Wesley, 1994.

[45] J. Bloomenthal with C. Bajaj, J. Blinn, M.-P. Cani-Gascuel, A. Rockwood, B. Wyvill, and G. Wyvill, editors. *Introduction to Implicit Surfaces*. Morgan Kaufmann Publishers, San Francisco, 1997.

[46] B. Wyvill, C. McPheeters, and G. Wyvill. Animating soft objects. *The Visual Computer*, 2(4):235–242, 1986.

[47] B. Wyvill, C. McPheeters, and G. Wyvill. Data structure for soft objects. *The Visual Computer*, 2(4):227–234, 1986.

[48] S. Yoshimoto. Ballerinas generated by a personal computer. *Journal of Visualization and Computer Animation*, 3(2):55–90, 1992.